A HELICAL-COIL RESONATOR MAGNETICALLY COUPLED WITH MICROSTRIP TRANSMISSION LINE FOR EPR SPECTROSCOPY

Marek Mossakowski[1,2], Jan Koprowski[1]

[1] Akademia Górniczo-Hutnicza – University of Science and Technology, Department of Electronics, Al. Mickiewicza 30, 30-059 Kraków, Poland; koprowsk@agh.edu.pl

[2] Uniwersytet Jagielloński – Jagiellonian University, Faculty of Biotechnology, ul. Gronostajowa 7, 30-387 Kraków, Poland

This simple resonator consists of silver wire formed as coil of two turns. Compared to cavity resonators working in the same frequency band, our resonator is substantially smaller - 0.8 mm inner diameter and 0.2 mm wire diameter (AWG of 32). The coil is suspended over the microstrip supply line which is connected to EPR spectrometer. The whole apparatus is an X band EPR probe for biological tissue research. The main advantage of our project in this simple construction of the probe is the convenient resonator's coupling and supplying RF power by a microstrip line. Simulations and real measurements of electromagnetic field distribution revealed impressive symmetry and an enormous magnetic field concentration along resonator's main axis where tissue samples are placed. The Λ factor for this resonator is over $20\,\mathrm{Gs}/\sqrt{\mathrm{W}}$. Analysis of resonance circuit shows a very wide resonance band (small quality factor – about 300). This is the desired feature in pulse EPR spectroscopy.

Keywords: *EPR spectroscopy, microstrip circuits, microwave resonators*

1. INTRODUCTION

Electron paramagnetic resonance (EPR) is the process of resonant absorption of microwaves by paramagnetic atoms or molecules, with at least one unpaired electron spin, and in the presence of a static magnetic field B_0 (Fig. 1). The great majority of EPR spectrometers is working at $B_0 \approx 34$ T (*X* band) or $B_0 \approx 1.25$ T (*Q* band).

The resonators (also qualified as cavities or probeheads) connected to the microwave bridge are the most important parts of EPR spectrometers (Fig. 2).

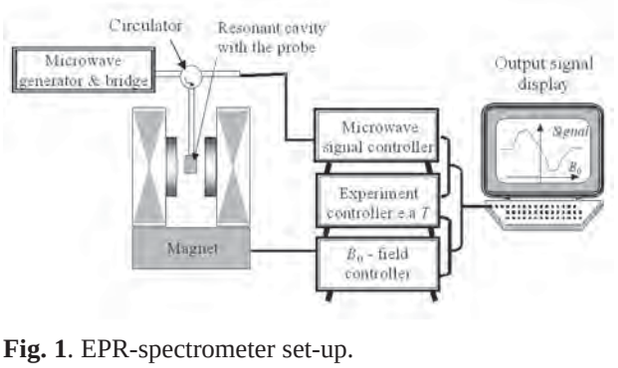

Fig. 1. EPR-spectrometer set-up.
Rys. 1. Budowa spektrometru EPR.

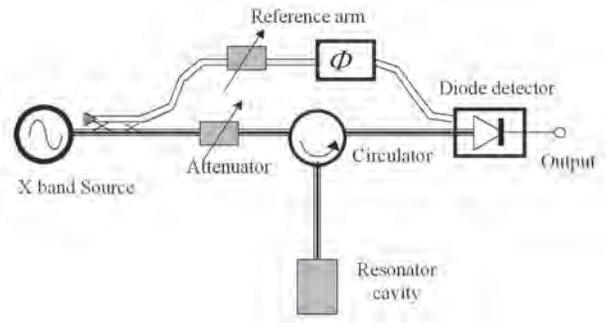

Fig. 2. Microwave signal path in EPR spectrometer.
Rys. 2. Tor mikrofalowy w spektrometrze EPR.

In spectrometers built on rectangular the waveguides, resonators are critically coupled with the transmission line by an adjustable hole in one of the cavity's wall or adjustable rod screwed into the waveguide close to the cavity's entrance. The microwave magnetic flux density *b* can be written as:

$$b(z,t) = b_m e^{\mathrm{j}(\omega t - k_{0z} z)} \tag{1}$$

where: b_m is the amplitude of the harmonic magnetic flux density orthogonal to B_0, ω the signal pulsation, $k_{0,z} = 2\pi/\lambda_0$ - the wave number in the *0z* direction of propagation. The absorption of microwaves begins in the resonator cavity pertially filled with a tested simple of the volume V_{prob} (Fig. 2).

During absorption, coupling with a partially filled resonator becomes not critical. Part of the delivered microwave energy is reflected and can be measured. Therefore, the performance of these resonators must

be carefully tuned to the overall system's capacity to operate effectively at low or high modulation frequencies and amplitudes, low and high microwave power, and for lossy samples such as water or biological tissue probes.

The quality factor of the resonator is defined as:

$$Q_1 = \omega \frac{W}{P_0} = \omega \frac{\frac{1}{2\mu_0} \int_{V_{resonator}} b^2 dV}{P_0} \qquad (2)$$

where: W is the magnetic energy stored in the resonator, μ_0 - the magnetic permeability of free space ($\mu_0 = 4\pi \times 10^{-7}$ H/m), P_0 - the incident microwave power.

Generally, a higher Q_1 means higher sensitivity. However in pulse applications high Q_1 is not desired because increases measurement dead time. There is also a need to consider the cavity's filling factor and the quality of the microwave source. The filling factor is the ratio of the integral of the microwave field over the sample volume relative to the integral of the total microwave field in the cavity:

$$\eta = \frac{\int_{V_{probe}} b^2 dV}{\int_{V_{resonator}} b^2 dV} \qquad (3)$$

For pulse and continuous wave applications there is another important parameter Λ - the resonator efficiency defined by the equation [4]:

$$\Lambda = \frac{B}{\sqrt{P_0}} \left[Gs / \sqrt{W} \right] \qquad (4)$$

where B_1 is the maximum available microwave flux density for a given incident microwave power [3]. At higher Λ factor the microwave source can have lower output power which also permits minimizing dead time in pulse spectroscopy

The volume of resonator's cavity is much bigger than the volume of samples. Thus in a modern EPR spectroscopy other resonator constructions are used and developed as helical, ceramic and loop gap resonators (LGR). The helical resonators have much smaller dimensions compared to the wavelength in the measurement system, called as microcoil-based probes or microresonators. They have high value of η.

2. EXPERIMENTAL

The microresonator, projected and built to our experiments, consists of the coil with the number of turns N = 2, diameter α = 0.8 mm and length l = 0.3 mm, mounted on the low-loss PCB (*Printed Circuit Board)* (Fig. 3a).

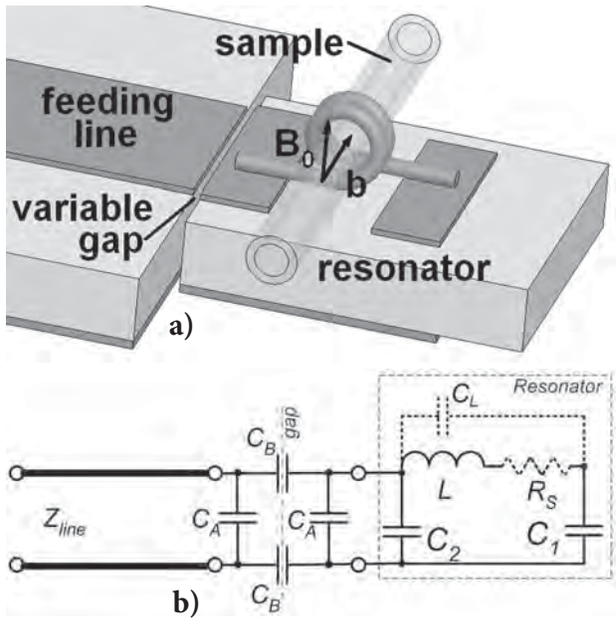

Fig. 3. Helix resonator electrically coupled with microstrip line: a) electrical coupling with the resonator; b) equivalent circuit diagram.

Rys. 3. Rezonator sprzężony polem elektrycznym z linią mikropaskową: a) rysunek poglądowy; b) schemat zastępczy.

For estimation purposes we used the inductance formula:

$$L \approx \frac{(aN)^2}{0.45a + l} \quad [\text{nH}] \qquad (5)$$

which is valid for $l \geq 0.4\,\alpha$ and all dimensions provided in [mm] [2]. Because of used winding technique, final relation between dimensions is l = 0.375 α. According to the formula (5) the inductance L = 3.88 nH, which is acceptable comparing to FEM simulator result L = 3.92 nH.

The self resonance frequency for LC circuit is defined as:

$$f_o = \frac{1}{2\pi \sqrt{LC_1}} \qquad (6)$$

For the coil without additional capacitors the resonance frequency is observed at the 23.5 GHz. This gives the capacitance between two coil's wires $C_L \approx 0.012\ C$ pF.

The inter-turns capacitance of the coil has a very small value and the main part of total capacitance is shared by two mounting pads of the microcoil resonator. Its capacitances are marked by C_1 and C_2 as shown in Fig. 3b. and Fig. 4b. Because of additional capacitances, the resonance frequency could be decreased to about 9.5 GHz.

The equivalent series resistance R_S of the coil at the frequency f_0 is:

$$R_S = \frac{d}{4\delta_s} R_{DC} \tag{7}$$

where δ_s is the skin depth. For two turns of silver wire of d = 0.2 mm, R_{DC} = 2.62 mΩ and R_S = 202 mΩ (for σ(Ag) = 61.10^3 S/mm and δ_s = 0.64 μm at 10 GHz). This value and the former solved data allows us, using the equation [4]:

$$Q_0 = \frac{\omega L}{R_S} \tag{8}$$

to estimate the two-turns coil's quality Q_0 = 573.

According the general microwave circuit theory of resonators [5]:

$$Q_L = \frac{Q_0}{1+\beta} \tag{9}$$

where β is the coupling coefficient of the resonator with supply line.

Pads under the coil were created by etching away a copper from 0.2 inch thick microwave laminate (ROGERS® 5880). They are used are to fix the main part of the resonator and to tune resonance frequency. Very small diameters and sample volume has allowed to obtain a very high Λ factor – over 20 Gs/√W. Small dimensions of the resonator evoke coupling problems because of very low values of lumped elements. Each pad under the coil has area of 0.8 mm x 2.4 mm and the both introduce two additional capacities $C_1 = C_2$ = 0.05 pF. The coil has the very low inductance L and self-capacitance C_L between the wire turns. The first successful attempt of coupling the microresonator with supply line was made by two series capacitors – coupling by electric field. Estimated values of capacitors C_A and C_B were about 0.01 pF. Such a small capacitance could be achieved only by leaving an air gap between the substrates with the microstrip line and the resonator (Fig. 3b). By adjusting the width of the gap we have a full control of the coupling factor. However, during experiments some construction imperfections were discovered:

- Changing gap's width caused C_2 capacity change, which provided significant changes of the resonance frequency during coupling process.
- Significant influence of mechanical precision to capacity changes of C_A and C_B. For example 10% variation was caused by a 50-μm sweep what in the next step resulted in the loss of critical coupling.
- Significant microwave leakage by the gaps forced to extend shield from resonator onto the gap.

Results of experiments with electric field coupling inspired us to apply magnetic coupling between the microstrip line and coil microresonator (Fig. 4).

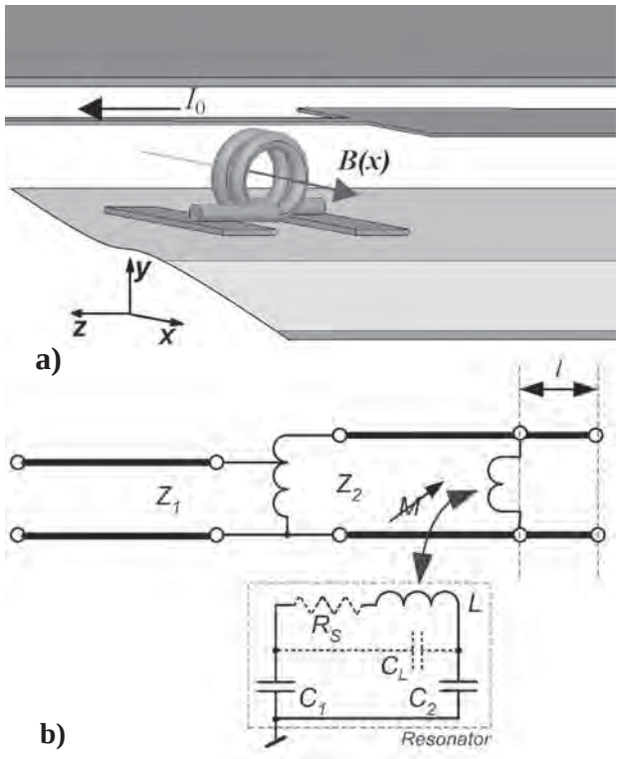

Fig. 4. Magnetically coupled helix resonator with microstrip line: a) microcoil-resonator above the microstrip line; b) equivalent circuit diagram.

Rys. 4. Rezonator sprzężony polem magnetycznym z linią mikropaskową: a) rysunek poglądowy; b) schemat zastępczy.

The next solution also is not mechanically complex and very easy to make (Fig. 5).

Feeding microstrip line is in the same distance to the coil during coupling process what practically means that all physical dimensions around coil are constant, which causes better stability of lumped elements in an equivalent circuit. We exploited field pattern of TEM mode in the microstrip line and the resonator was placed in the way that its axis is parallel to magnetic field lines, generated by the coupled microstrip line. The coil is suspended over the microstrip supply line (Figs. 5 – 6).

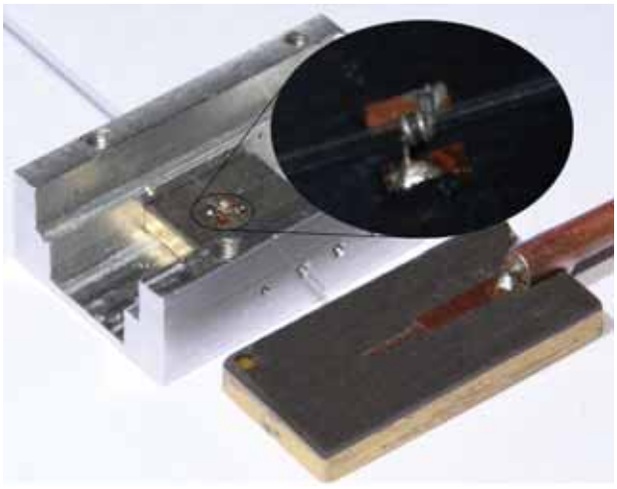

Fig. 5. Decomposed resonator with magnetic coupling.
Rys. 5. Rozłożony rezonator sprzężony magnetycznie.

The microstrip line, placed directly under the resonator was narrowed-down to increase the density of microwave magnetic field lines. This procedure according to circuit analysis resulted in increasing the density of the surface current J_{sz}:

$$J_{sz}(x,z) = \frac{b(x)}{\mu_0} e^{-jk_{0z}z} \quad [\text{A/m}] \qquad (10)$$

along the line in the *0z* direction (Fig. 4a.).

The inductance of microstrip is also growing due to increasing the density of the magnetic flux $b(x)$ around the microstrip line [6]:

$$b(x) = \frac{\mu_0 I_m}{\delta\sqrt{\left(\frac{w}{2}\right)^2 - x^2}} \qquad (11)$$

where: I_m is the amplitude of the ac current in the microstrip, w – the width of the microstrip

The end part of 50-Ωm transmission line was narrowed-down 10 times. Its open end assures the boundary condition $b = 0$. The length of narrowed-down part of the line is in the range of $\lambda_0 / 4 < L < \lambda_0$. The coupling point is situated at a distance l from the end of the line (Fig. 4b).

3. RESULTS

Simulations made on Ansoft® HFSSvs10 were helpful to illustrate very precisely the magnetic field distribution near the coupling point (Fig. 6).

The colours on the diagram provide us the magnetic field intensity from 20 Gs (red) down to 0.2 Gs (green). The scale is logarithmic. On this pattern of the magnetic field inside the microresonator, there are shown very clear interactions between a quasi-TEM mode of the microstrip line and the inducted magnetic field. *In situ* measurements of S_{11} parameter of the magnetically coupled microresonator were made using a vector network analyzer, HP8720C (Fig. 7).

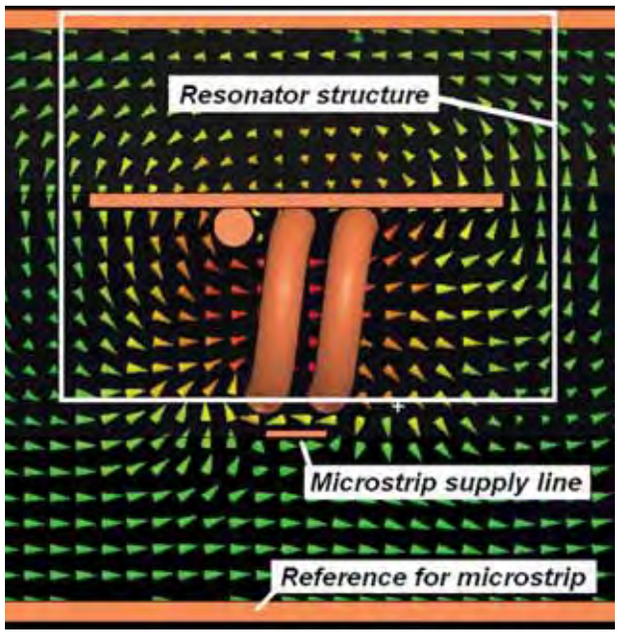

Fig. 6. Visualization of microwave magnetic field in resonator.
Rys. 6. Kształt pola magnetycznego w rezonatorze.

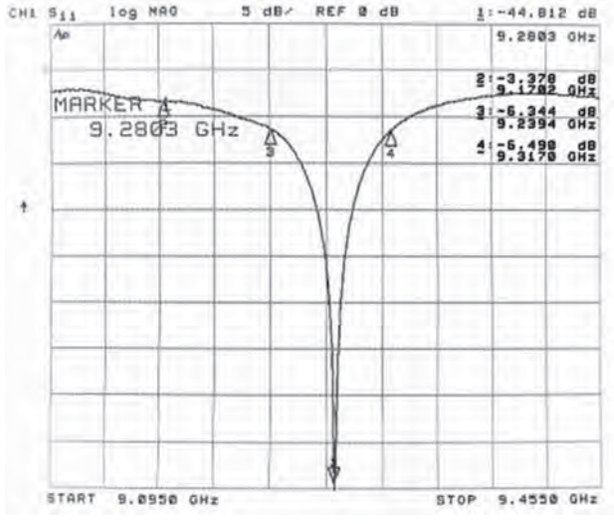

Fig. 7. Resonator response.
Rys. 7. Odpowiedź rezonatora.

The 3-dB bandwidth Δf_{3dB} = 77 MHz and resonant frequency f_0 = 9.28 GHz, directly readout from the resonance curve, gives Q_0 = 241.

4. DISCUSSION

The results of the al built-in resonator measurements, the electromagnetic (EM) field simulation in the resonator and its lumped element equivalent circuit simulation are compared in Fig. 8. In the EM simulation, all dimensions and electro magnetic parameters of actual resonator were taken into account. Lumped elements were estimated using equations presented in this paper. The level of additional insertion losses is about 3 dB. These insertion losses are noticeable in the results measurements of the actual construction of the resonator and in the results from the EM simulator. The lack of additional insertion losses in the results from the circuit simulator infers that in the equivalent circuit an additional lossy lumped element should be included.

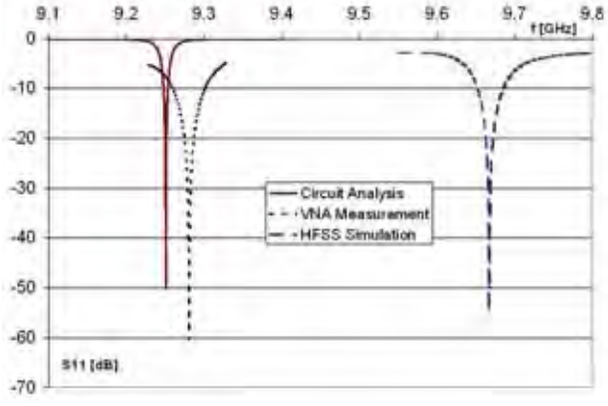

Fig. 8. Comparison of measured and calculated characteristics of S_{11} and f_0.resonator parameters.
Rys. 8. Porównanie zmierzonych i obliczonych charakterystyk parametrów rezonatora S_{11} i f_0.

The resonant frequency of the actual resonator is different in comparison to that one provided by the EM simulations. The error is about 4%. The error of the resonant frequency provided by the equivalent circuit simulations is about 4.3% compared to the EM simulation.

At critical coupling (β = 1 in eqn. (9)), a quality of the loaded resonator is:

$$Q_{Loaded} = \frac{\omega L}{2R_S} \tag{12}$$

Analysing current induced by the incident microwave power P_0 in the turns with series resistance R_S, we may state that the amplitude of the microwave field inside the coil of length l is:

$$B_1 \simeq \mu_0 \frac{N}{l}\sqrt{\frac{2P_0}{R_S}} \tag{13}$$

And following the equation (12), we express it as:

$$B_1 \simeq \mu_0 \frac{2N}{l}\sqrt{\frac{Q_L}{\omega L}P_0} \tag{14}$$

This equation allows us to define and understand the Λ coefficient:

$$\Lambda \cong \frac{B_1}{\sqrt{P_0}} \cong \mu_0 \frac{2N}{l}\sqrt{\frac{Q_L}{\omega L}} \tag{15}$$

It can be written in the CGS system as the formula (4).
So, at microwave power 1 W supplied to the two-turns resonator with Q_L = 308 we introduce to the microcoil a magnetic field B_1 = 20.04 Gs to get Λ = 20.04 Gs/√W. The accurate values of the magnetic field and Λ factor were obtained using the simulator based on the implementation of finite elements method to electromagnetic calculations.

5. CONCLUSION

Our investigations open new possibilities in adaptation of the helical microresonators for EPR spectroscopy working in X band frequencies. The analysis of the resonator equivalent circuit, based on lumped elements and transmission lines, provides characteristic parameters of the microresonator. Statements of the results are simple for interpretation and should be helpful in designing of the helical microresonators for EPR spectroscopy.

ACKNOWLEDGEMENT

The Authors would like to thank Prof. Wojciech Froncisz from Jagiellonian University, Ph.D. James Hyde and M.Sc. Jason Sidabras from Medical College of Wisconsin for inspirations and first common experiments with such a microresonator undertaken during the short stage at Medical College of co-author Marek Mossakowski.

REFERENCES

[1] Lurie D.J.*:* Techniques and applications of EPR imaging, *Electron Paramagnetic Resonance*, 18, RSC, ed. The Royal Society of Chemistry, 2002

[2] Vizmuller P.: RF design guide: systems, circuits, and equations, ARTECH HOUSE Inc., 1995, 218-219

[3] Hyde J.S., Froncisz W.: Advanced EPR: Applications in biology and biochemistry, ed. by A. J. Hoff, Amsterdam, ELSEVIER, 1989, 277-306

[4] Sadiku M.N.O.: Elements of electromagnetics, *Oxford University Press* 2001, 428

[5] Galwas B.: Wielowrotniki i rezonatory mikrofalowe, Wydawn.Politechniki Warszawskiej, 1985

[6] Wadell B.C.: *Transmission line design book;* Artech House Inc. 1991

REZONATOR HELIKALNY SPRZĘŻONY MAGNETYCZNIE Z LINIĄ MIKROPASKOWĄ DO ZASTOSOWAŃ W SPEKTROSKOPII EPR

Opisany rezonator zbudowany został ze srebrnego drutu o średnicy 0.2 mm uformowanego w dwuzwojową cewkę o wewnętrznej średnicy 0.8 mm. W porównaniu do rezonatorów wnękowych pracujących w tym samym zakresie częstotliwości, przedstawiony rezonator helikalny stanowi niewielki ich ułamek objętości. Cewka jest zawieszona nad linią mikropaskową podłączoną do mostka mikrofalowego spektrometru EPR. Rezonator zbudowany został z przeznaczeniem do badań uwodnionych próbek biologicznych w paśmie X. Głównym zamierzeniem autorów było udoskonalenie sprzężenia rezonatora z mikropaskową linią zasilającą. Przeprowadzone symulacje i rzeczywiste pomiary rozkładu pola elektromagnetycznego ujawniły dużą symetrię i olbrzymią koncentrację pola magnetycznego wzdłuż głównej osi rezonatora, w miejscu gdzie znajduje się badana próbka. Współczynnik Λ dla opisanego rezonatora przewyższa wartość 20 GS/√W, natomiast pasmo rezonansowe jest bardzo szerokie – mała dobroć układu ~ 300. Powyższe cechy rezonatora są pożądane w impulsowej spektroskopii EPR.

Słowa kluczowe: rezonator EPR, sprzężenie magnetyczne, rezonator helikalny

NOWE KOMPOZYTY GRUBOWARSTWOWE O OBNIŻONEJ TEMPERATURZE SPIEKANIA PRZEZNACZONE NA KONTAKTY OGNIWA SŁONECZNEGO

Anna Młożniak[1)], Piotr Ungier[2)], Małgorzata Jakubowska[1,2)]

[1)] Wydział Mechatroniki, Politechnika Warszawska, ul. Św. Andrzeja Boboli 8, 02-525 Warszawa, e-mail: maljakub@mchtr.pw.edu.pl

[2)] Instytut Technologii Materiałów Elektronicznych, ul. Wólczyńska 133, 01-919 Warszawa e-mail: maljakub@itme.edu.pl

W pracy przedstawiono nowa generację materiałów grubowarstwowych przeznaczonych do nanoszenia sitodrukiem, w których fazę przewodzącą stanowią proszki srebra o submikronowej wielkości ziaren. Zaletą tych past jest to, że nie zawierają fazy szkliwa, które wspomagało proces spiekania, a jednocześnie pogarszało przewodnictwo elektryczne warstwy. Kolejna zaleta tych past to możliwość spiekania w niższych temperaturach, co zwieksza obszar stosowania tych past w róznych procesach technologicznych

Słowa kluczowe: technologia grubowarstwowa, nanoproszek srebra, ogniwo słoneczne

1. WSTĘP

Dotychczas stosowane pasty srebrowe do technologii grubowarstwowej przeznaczone do nanoszenia na podłoża techniką sitodruku składały się z fazy przewodzącej, którą stanowił proszek srebra